CARDIFF UNIVERSITY
PRIFYSGOL CAERDYDD

ORCA – Online Research @ Cardiff

This is an Open Access document downloaded from ORCA, Cardiff University's institutional repository:https://orca.cardiff.ac.uk/id/eprint/114596/

This is the author's version of a work that was submitted to / accepted for publication.

Citation for final published version:

Yi, Lok, Frentrup, Martin, Kappers, Menno, Oliver, Rachel, Humphreys, Colin and Wallis, David 2018. Effect of growth temperature and V/III-ratio on the surface morphology of MOVPE-grown cubic zincblende GaN. Journal of Applied Physics 124 , 105302.

Publishers page: http://dx.doi.org/10.1063/1.5046801

Please note:
Changes made as a result of publishing processes such as copy-editing, formatting and page numbers may not be reflected in this version. For the definitive version of this publication, please refer to the published source. You are advised to consult the publisher's version if you wish to cite this paper.

This version is being made available in accordance with publisher policies. See http://orca.cf.ac.uk/policies.html for usage policies. Copyright and moral rights for publications made available in ORCA are retained by the copyright holders.

Effect of growth temperature and V/III-ratio on the surface morphology of MOVPE-grown cubic zincblende GaN

Lok Yi Lee[1, *], Martin Frentrup[1], Menno J Kappers[1], Rachel A Oliver[1], Colin J Humphreys[1,2] and David J Wallis[1,3]

[1] Department of Materials Science and Metallurgy, University of Cambridge, 27 Charles Babbage Road, Cambridge, CB3 0FS, United Kingdom

[2] School of Engineering and Materials Science, Queen Mary University of London, London, E1 4NS, United Kingdom

[3] Centre for High Frequency Engineering, University of Cardiff, 5 The Parade, Newport Road, Cardiff, CF24 3AA, United Kingdom

[*] Corresponding author: lyl24@cam.ac.uk

Abstract

The influence of growth temperature and V/III-ratio on the surface morphology of (001) cubic zincblende GaN epilayers during metal organic vapour phase epitaxy (MOVPE) growth has been investigated using atomic force microscopy (AFM) and transmission electron microscopy (TEM). The zincblende phase purity as determined by X-ray diffraction (XRD) was found to be above 98 % for most GaN epilayers studied. As the growth temperature was increased from 850 °C to 910 °C, and as the V/III-ratio was separately increased from 38 to 300, surface features were found to be elongated in [1-10] direction, and the ratio of the length to width of such surface features was found to increase. Faceting was observed at V/III-ratios below 38 and above 300, which in the latter case was accompanied by a reduction of the zincblende phase purity. An explanation for these morphological trends is proposed based on effects such as the reduced symmetry of the top monolayer of the (001)-

oriented zincblende GaN lattice, diffusion of Ga and N adatoms on such a surface, and the relative energies of the crystal facets.

Keywords: cubic zincblende GaN, MOVPE, morphology, surface roughness, growth model

1. Introduction

After its initial synthesis by Mizuta *et al.* in 1986 [1], cubic zincblende GaN (zb-GaN) received significant attention in the subsequent 15 or so years [2,3] before research efforts dwindled to that of only a handful of research groups [4–9]. However, due to its potential to overcome the 'green gap' problem, there has been renewed interest in zincblende III-nitrides with the recent demonstration of green light-emitting InGaN/GaN quantum well structures [10–12]. Due to the non-polar nature of the zincblende crystal structure, the spontaneous and piezoelectric polarisation fields, which result in the quantum-confined Stark effect in the hexagonal wurtzite (wz) crystal structure, are absent in the zincblende [001] growth direction [13,14]. Furthermore, the smaller band gap of zb-GaN (3.27 eV) compared with that of wz-GaN (3.47 eV) allows longer wavelength emission to be achieved for a smaller indium content in the active region of InGaN/GaN devices compared with equivalent non-polar or semi-polar wurtzite structures, and would be especially advantageous for green-emitting devices. However, zb-GaN films with high phase purity are difficult to grow since the zincblende structure is metastable, and stacking faults and inclusions of the thermodynamically more stable wurtzite phase commonly occur [15–17].

Although growth of zincblende III-nitrides is possible using overgrowth of patterned Si (100) substrates with {111} side walls, this approach results in stripes of zb-GaN crystal [10,11] rather than the growth of a continuous planar film. A method which allowed the growth of planar

films on large-area substrates that are readily-available would be much more attractive. A few groups reported the growth of zb-GaN on GaAs (001) substrates by molecular beam epitaxy (MBE) [18–20] and metalorganic vapour phase epitaxy (MOVPE) [21,22], but the high thermal stability of 3C-SiC substrates is preferable because of the relatively high temperatures required for GaN growth [23–25]. Moreover, 3C-SiC has a relatively small lattice mismatch of 3.4 % with respect to zb-GaN [26], and the current availability of high-quality 3C-SiC/Si(001) substrates of up to 150 mm in diameter presents a promising choice of substrate for zb-GaN films. A comparison of the MOVPE conditions studied by the different groups [23–25] indicates that the highest quality films were grown using a two-step growth procedure similar to that normally used on (0001) sapphire, which included a thin low-temperature GaN nucleation layer, followed by high temperature epilayer growth.

In the absence of a comprehensive MOVPE growth study of zb-GaN, we report on the effect of growth temperature and V/III-ratio on the surface morphology of zb-GaN grown on 3C-SiC/Si substrates with a 4° or 0° miscut. We analyse the size of surface features using AFM, and propose a model for the distinct growth regimes observed. The model considers the anisotropy of in-plane strain, reduced symmetry of the top monolayer of the (001)-oriented zb-GaN lattice, the diffusion of Ga and N adatoms on such a surface, and the relative energies of crystal facets.

2. Experimental

The GaN epilayers were grown by MOVPE in a 6 × 2” Thomas Swan close-coupled showerhead reactor on ~ 2 × 2 cm^2 pieces of a 150 mm diameter (001) 3C-SiC/Si substrate provided by Anvil Semiconductors Ltd. The substrate consists of a 2.9 µm thick layer of 3C-SiC grown on a 1000 µm thick Si wafer with either 4° or 0° miscut towards the [110] in-

plane direction. Thin GaN nucleation layers were grown on pieces of the 3C-SiC/Si substrate, followed by ~ 300 nm thick GaN epilayers grown under a range of growth temperatures and V/III-ratios. The Ga and N sources were trimethylgallium (TMG) and ammonia (NH_3) respectively, and hydrogen was used as the carrier gas.

Two series of samples were grown to investigate the influence of the MOVPE growth temperature and V/III-ratio in the gas phase. For the growth temperature series, six samples were grown at temperatures ranging from 850 °C to 910 °C at a constant V/III-ratio of 76. For the V/III-ratio series, eight samples were grown at V/III-ratios ranging from 15 to 1200 at a fixed growth temperature of 875 °C. The variation in V/III-ratio was achieved by keeping the gas flow of TMG into the reactor constant, while the gas flow of ammonia was adapted for each growth run.

The GaN surface morphologies were measured ex-situ using a Digital Instruments Dimension 3100 atomic force microscope (AFM) in tapping mode. MPP-11100-10 tips from Bruker Nano Inc. with a nominal tip radius of 8 nm were used. The topographic data obtained from the AFM was analysed using the free software package WSxM [27]. The fast scan direction for the samples grown on a 4° miscut substrate is along [110], unless otherwise stated. The image height (H) stated in the caption of each AFM scan is the height range from black to white in the image.

To quantify the typical sizes of the surface features along [110] and [1-10], which correspond to directions parallel and perpendicular to the miscut direction of the off-axis substrate, we used the two-dimensional fast Fourier transform (2D-FFT) of the AFM scans. First, we applied a 2D-FFT filter to each 10 × 10 μm^2 AFM scan. Then we extracted the intensity

profile from the centre of the 2D-FFT pattern in the [110] and [1-10] direction. The intensity profile typically followed a Gaussian distribution curve, from which we obtained the full width at half maximum (FWHM). The reciprocal of the FWHM gives a measure of the average feature size along [110] and [1-10], defined as $f_{[110]}$ and $f_{[1\text{-}10]}$ respectively. This procedure was repeated for five different areas on the surface of each sample, and the five measurements were averaged. The standard error of the mean from the five measurements was used to define the error bars of our measurements.

The facets present on the surface of the samples grown at V/III-ratios of 300 and 1200 were examined in more detail by cross-sectional bright-field transmission electron microscopy (TEM) imaging, using a Tecnai F20 operated at 200 kV.

As growth conditions and faceting could both significantly influence the crystal quality, we have also measured the phase purity of the samples by X-ray diffraction (XRD) using a PANalytical Empyrean diffractometer equipped with a two-bounce hybrid monochromator (λ = 1.54056 Å), 1/4° primary beam slit, and a PIXcel solid-state area detector. Reciprocal space maps of the 113 zb-GaN reflections with their stacking fault related intensity streaks were collected in asymmetric geometry, and subsequently the intensity profiles along the streaks (Q ∥ [111]), such as Figure 1, were extracted from the reciprocal space maps. Pseudo-Voigt functions for the zincblende and wurtzite phases were fitted to the intensity profile at the theoretical positions of ~ 4.03 Å and ~ 3.64 Å, respectively. A third Pseudo-Voigt function was fitted in between the zincblende and wurtzite fits to consider the contributions from highly defective zb-GaN regions, containing bunches of stacking faults. The integrated intensities of these fits were then used to quantify the proportion of each phase.

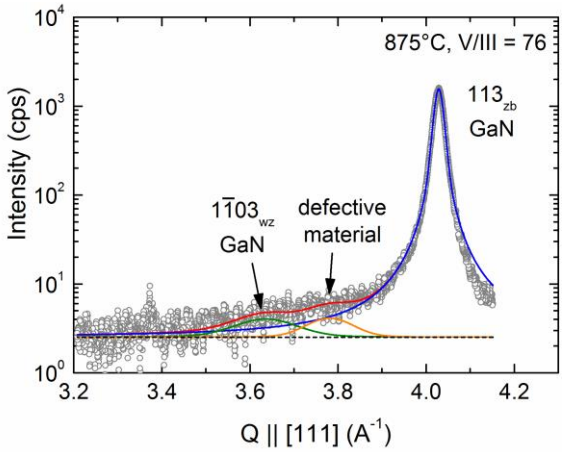

Figure 1 XRD intensity profile through the 1-103_{wz} and 113_{zb} reflections (grey circles) for the sample grown on a 4° miscut substrate at 875°C and a V/III-ratio of 76. Pseudo-Voigt fits for the zb-phase (blue), wz-phase (green), and defective zb-GaN material (orange) were used to estimate the phase fractions.

3. Results and discussion

3.1. Effect of substrate miscut

Recent work by Kemper *et al.* [28] highlighted the deleterious effect of antiphase domain boundaries on the surface morphology and phase purity of zb-GaN epilayers grown on on-axis 3C-SiC/Si substrates. It is well known that the presence of antiphase domains (APDs) in compound semiconductors on Si can be suppressed by introducing a miscut of $\lesssim 5°$ to the Si substrate [29]. Therefore, the effect of the substrate miscut on the surface morphology was first determined by comparing the AFM images of zb-GaN epilayers grown on two different substrates with nominally 0° and 4° miscut in [110] direction under typical conditions and in the same growth run, as shown in Figure 2 (a) and (b), respectively.

The GaN epilayer grown on the on-axis substrate (Figure 2 (a)) has distinct domains of elongated surface features, with neighbouring domains having surface features that are

aligned along two perpendicular <110> directions. This indicates the presence of two types of domains which we ascribe to the presence of APDs. In contrast, the GaN epilayer grown on the 4° miscut substrate (Figure 2 (b)) shows surface features aligned only along one direction, [1-10], indicating that the APDs have been suppressed. The AFM scan of the bare on-axis 3C-SiC/Si substrate in Figure 2 (c) reveals meandering boundaries, highlighted in red in Figure 2 (d), which we believe are further evidence of antiphase domain boundaries in the 3C-SiC layer, although the as-grown surface morphology of the 3C-SiC is lost due to a chemical mechanical polish process prior to zb-GaN growth. In view of these results, substrates with a 4° miscut along [110], free of APDs, were used for the rest of the study.

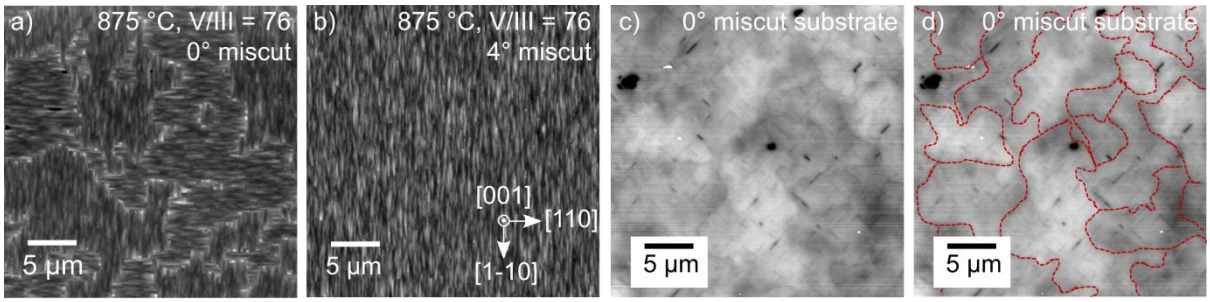

Figure 2 (a) AFM scan of a zb-GaN surface grown on a substrate with 0° miscut. H = 210 nm. (b) AFM scan of a zb-GaN surface grown on a substrate with 4° miscut. H = 105 nm. Both samples in (a) and (b) were grown at 875 °C and V/III-ratio of 76. (c) AFM scan of the on-axis (001) 3C-SiC/Si substrate, and (d) the same image as (c) with the meandering boundaries highlighted. H = 7 nm.

3.2. Effect of growth temperature

The change in surface morphology of the GaN epilayer with growth temperature is shown in the AFM scans in Figure 3Figure 3. As the temperature was increased from 850 °C to 910 °C, the geometry of the surface features changes from elongated along [1-10] to become more square-like. This observation is reflected in the average feature sizes extracted from the

AFM height data using the method described in Section 2. Figure 4Figure 4 (a) reveals that the feature size in [110] direction ($f_{[110]}$) increases by a factor of two from (0.64 ± 0.04) µm to (1.31 ± 0.09) µm as the growth temperature increases from 850 °C to 910 °C. In contrast, the feature size in [1-10], ($f_{[1\text{-}10]}$) in Figure 4 (b), is approximately halved from (3.75 ± 0.38) µm to (2.08 ± 0.11) µm in the same increasing temperature range. Consequently, the aspect ratio ($f_{[1\text{-}10]}/ f_{[110]}$) decreases from 5.8 ± 0.7 (elongated) to 1.6 ± 0.1 (square-like) with increasing temperature as shown in Figure 4 (c). The root mean square (rms) surface roughness of 10 x 10 μm^2 AFM scans in Figure 4 (d) ranges from (10.4 ± 0.1) nm to (12.9 ± 0.3) nm, which is not a significant variation. The lowest rms roughness is observed at a growth temperature of 885 °C, which is in the middle of the temperature range investigated. Such rms roughness values are in the same order of magnitude as reported for semi-polar (11-22) GaN growth on sapphire, where similar surface undulations were observed [30]. The zb-GaN content determined by XRD is shown in Figure 5, which indicates that the zincblende content of all samples was above 98 %, with only a small deterioration in phase purity for growth temperatures above 885 °C.

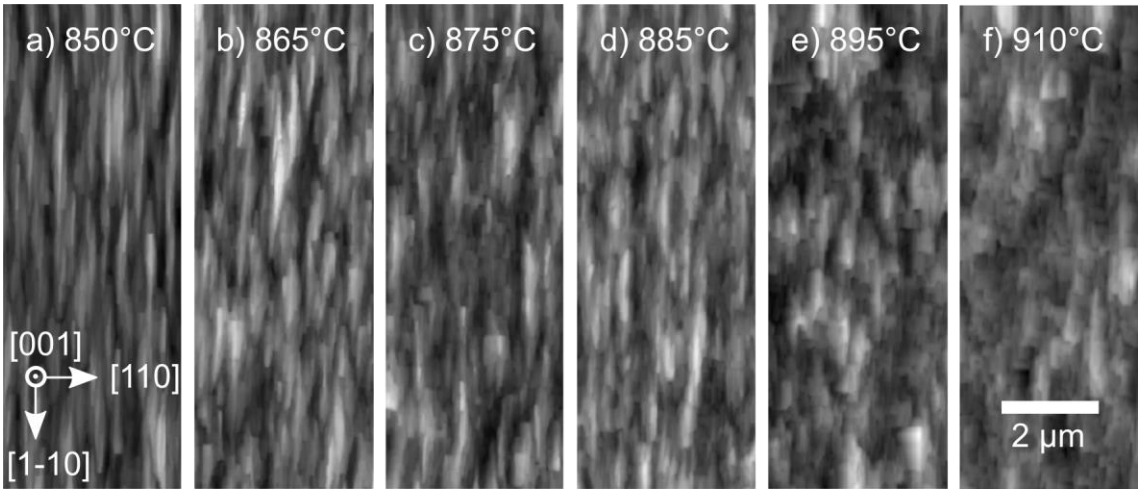

Figure 3 AFM scans of the surfaces of zb-GaN epilayers grown at varied growth temperatures and a constant V/III-ratio of 76. The growth temperature used is indicated at the top of each image. From (a) – (f), H = 117 nm, 85 nm, 90 nm, 72 nm, 79 nm and 103 nm.

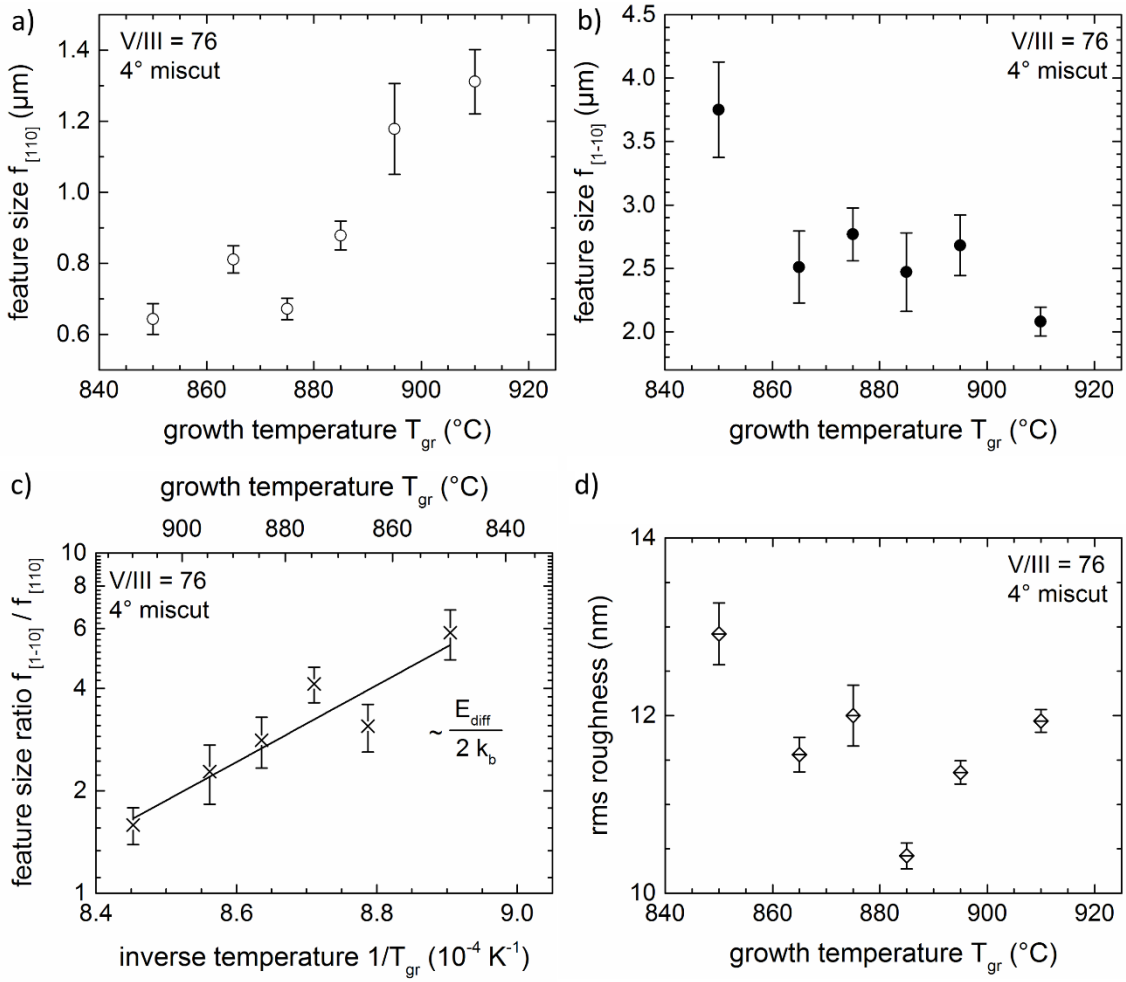

Figure 4 Feature sizes in (a) [110] and (b) [1-10] directions extracted from 2D-FFT of AFM height data of zb-GaN epilayers grown at different growth temperatures and a constant V/III-ratio of 76. (c) Variation of the aspect ratio of surface features with growth temperature. The function $y = A \exp\left(\frac{E_{diff}}{2k_b} \cdot \frac{1}{T}\right)$ was fitted as shown by the line of best fit. (d) Variation of root mean square surface roughness with growth temperature.

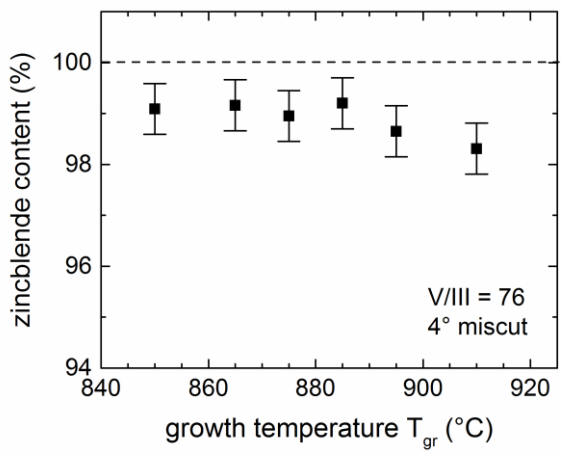

Figure 5 Zb-GaN content determined by XRD as a function of the GaN epilayer growth temperature.

A similar surface morphology with elongated surface features is observed in both the zb-GaN film grown on a 4° miscut substrate and within an APD of the zb-GaN film grown on a 0° miscut substrate (Figure 2). This demonstrates that the surface morphology seen in the samples grown on a 4° substrate is not simply related to step-bunching driven by the substrate miscut, but must be determined by surface energy considerations. The 90° rotation of the surface morphology in neighbouring APDs of a zb-GaN film grown on a 0° miscut substrate further suggests that the surface morphology is controlled by the symmetry of the crystal surface.

A common source of the periodic surface undulations observed is the self-organisation of the surface to minimise the thin film's total energy, given by its in-plane strain energy and surface energy. The surface atoms of the thin film redistribute to form periodic peaks and troughs, such that the in-plane strain is minimised at the cost of an increasing surface energy [31].

The striated GaN surface features observed indicate that the underlying diffusion process is anisotropic along the two in-plane directions, [110] and [-110]. For this behaviour, we have identified two possible causes for anisotropic diffusion on the surface: anisotropic in-plane strain as the driving force for the atom flux, and the reduced symmetry of the top monolayer of a (001)-oriented zb-GaN lattice.

For a (001) zb-GaN layer growing on a perfect (001) SiC/Si substrate, the lattice mismatch strain should be isotropic. However, in an earlier publication [26] we have shown that for a zb-GaN film grown on a 3C-SiC/Si substrate with 4° miscut towards [110], the in-plane strain in the [110] direction ($(3.65 \pm 0.11) \times 10^{-3}$) is slightly larger than that in the [1-10] direction ($(1.92 \pm 0.09) \times 10^{-3}$). We believe this small post-growth anisotropy in strain is related to plastic deformation of the Si substrate which occurs at the high temperatures used for growth of the SiC and results in a "pringle" shaped bowing of the wafers. Since this anisotropy in strain is small we do not believe that it contributes significantly to the surface morphology seen and this is supported by the fact that a similar morphology is observed within each APD for a zb-GaN film grown on the on-axis substrate, where the in-plane strains are isotropic. Nevertheless, we note that, based on the work of Gao and Nix [31], the anisotropy of in-plane strain we observe would lead to a larger degree of rearrangement per unit length along [110] than along [1-10], and consequently a shorter $f_{[110]}$ than $f_{[1\text{-}10]}$ as observed in our samples.

The schematic in Figure 6 shows the atomic arrangement of the Ga-N bilayers close to the surface of a (001)-oriented zb-GaN lattice, with (a) showing the top view of the (001) plane, and (b) the cross-sectional view along the [1-10] zone axis. The small and large circles represent the positions of Ga and N atoms, the red filled circles mark the atoms in the top-most monolayer, while the open circles show the underlying monolayer. It is clearly seen in

the projection of the (001) plane in Figure 6 (a) that the surface has a two-fold symmetry, with the alternating Ga and N atoms in the top monolayer arranged in chains, which run along the [1-10] direction and are separated by ½ of the unit cell face diagonal. The atoms in the monolayer directly below are arranged in the same way, but the -Ga-N- chains are shifted by ½ of the unit cell length with respect to the top monolayer. Based on this reduction in symmetry, it is not unreasonable to expect surface adatoms to have different diffusion coefficients in the [110] and [1-10] directions. Within our MOVPE reactor, it is not possible to obtain detailed information about any surface reconstructions at the growth surface such as that given by reflection high energy electron diffraction (RHEED) in MBE growth, but it is speculated that potential valleys, highlighted in yellow in Figure 6 (a) and (b), are present between the -Ga-N- chains in the top monolayer. Within such valleys, adatoms can easily diffuse between local surface potential minima, whereas diffusion across the -Ga-N- chains is hindered.

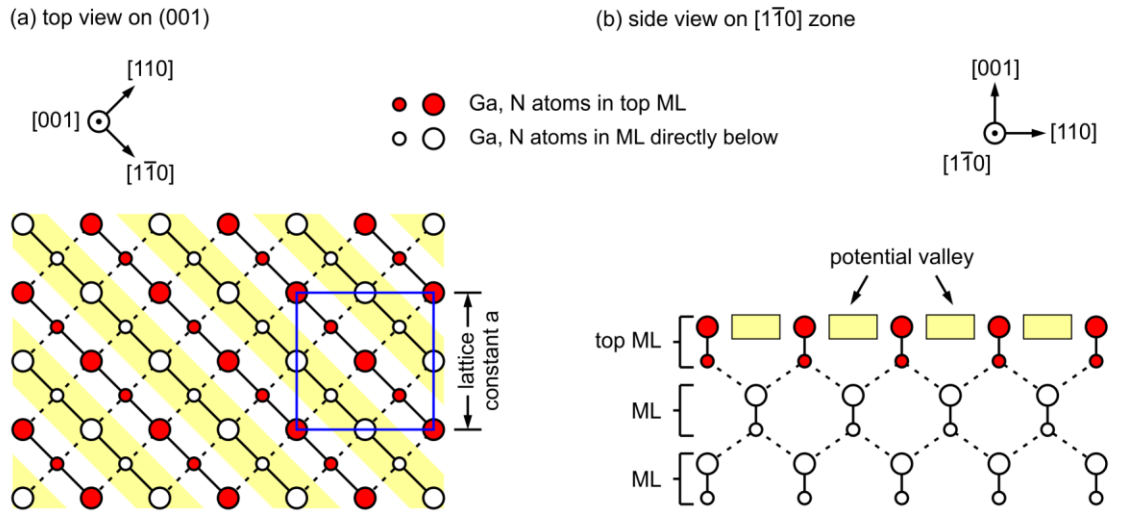

Figure 6 Arrangement of atoms of a (001)-oriented zb-GaN lattice. (a) Projection of the (001) plane, (b) cross-sectional view along the [1-10] zone axis. The blue square in (a) indicates the unit cell of zb-GaN.

In order to explain the evolution of the surface morphology, we propose that at relatively low growth temperatures, adatoms are likely to be trapped in the potential valleys, limiting diffusion along [110] and resulting in features being elongated along the potential valleys in the [-110] direction. With increasing temperature, it becomes more likely that adatoms can diffuse across the -Ga-N- chains, leading to the experimentally observed increase in $f_{[110]}$. We suppose that the activation of adatoms to diffuse across the -Ga-N- chains reduces the number of adatoms trapped in potential valleys for the diffusion within the valleys, thus explaining the reduction in $f_{[110]}$. Overall, the shape of the features becomes increasingly square-like at higher growth temperatures, as the diffusion along the two in-plane directions become more similar.

Based on the measured feature size change with growth temperature, the energy difference (E_{diff}) between the potential barriers for diffusion within the valley and across the -Ga-N- chains can be estimated. In a simplified model, the average diffusion length (λ) of an adatom at temperature (T) is given by the diffusion coefficient (D) and the average lifetime (τ) on the surface before it is incorporated into the lattice or desorbs: [32,33]

$$\lambda(T) \sim \sqrt{D\,\tau} = \sqrt{D_0\,\tau} \times e^{\frac{-\Delta E}{2k_bT}} \qquad \text{(Eq. 1)}$$

Here D_0 is the temperature independent diffusion constant and ΔE is the potential barrier energy. Using Eq. 1 and assuming that the feature sizes ($f_{[110]}$ and $f_{[1\text{-}10]}$) are proportional to λ, the ratio of the feature size in the [1-10] and [110] directions in Figure 4 (c) can be described by:

$$\frac{f_{[1-10]}}{f_{[110]}} \sim e^{\frac{-(\Delta E_{[1-10]}-\Delta E_{[110]})}{2k_bT}} = e^{\frac{-E_{diff}}{2k_bT}} \qquad \text{(Eq. 2)}$$

yielding the energy difference $|E_{diff}|$ = (4.3 ± 0.5) eV. Such a calculated potential barrier energy should be treated as an order of magnitude estimate, since the mathematics applied is not a complete solution of the diffusion equation, and furthermore, other processes including possible changes in the V/III-ratio with temperature may influence the morphology.

For non-polar a-plane and m-plane wz-GaN, Lymperakis *et al.* [32] calculated barrier energies between 0.21 eV and 0.93 eV, depending on the growth orientation and in-plane direction. Ploch *et al.* [34] measured barrier energies of ~ 0.8 eV and 1.3 eV for semi-polar (11-22) GaN. Our result on the difference between the activation energies in the two perpendicular directions suggest that the actual activation energies, particularly across the potential valleys in [110] direction, are relatively high in comparison to values in the literature for wz-GaN, and the difference is possibly due to the difference in the arrangement of atoms and dangling bonds between zb-GaN and wz-GaN. Brandt *et al.* [3] measured an activation energy of 2.48 eV for diffusion of Ga on (001) zb-GaN, which accords with our suggestion that the activation energies for diffusion may be relatively high in the zb-GaN system. However, it is unclear whether differences in the activation energy in different directions influenced Brandt *et al.*'s analysis.

3.3. Effect of V/III-ratio

Another important parameter that controls the surface morphology of (001) zb-GaN thin films is the V/III-ratio in the gas phase during MOVPE growth. Figure 7 shows AFM scans of the surface morphology of a series of samples grown at V/III-ratios ranging from 15 to 1200, at a fixed growth temperature of 875 °C. For the samples grown at the lower V/III-ratios the surface morphologies show a significant difference to that seen at higher V/III-ratios. For a V/III ratio of 15, the surface features are aligned along two axes, at ~ ± 45° from the [110] direction, as marked by the bold white arrows in Figure 7 (a). For samples grown at

a V/III-ratio of 38 and above (Figure 7 (c) – (h)), the surface morphologies consist of features elongated only along the [1-10] direction, similar to that observed in the temperature series. The sample grown at a V/III-ratio of 23 appears to be a transition between the two types of surface morphology.

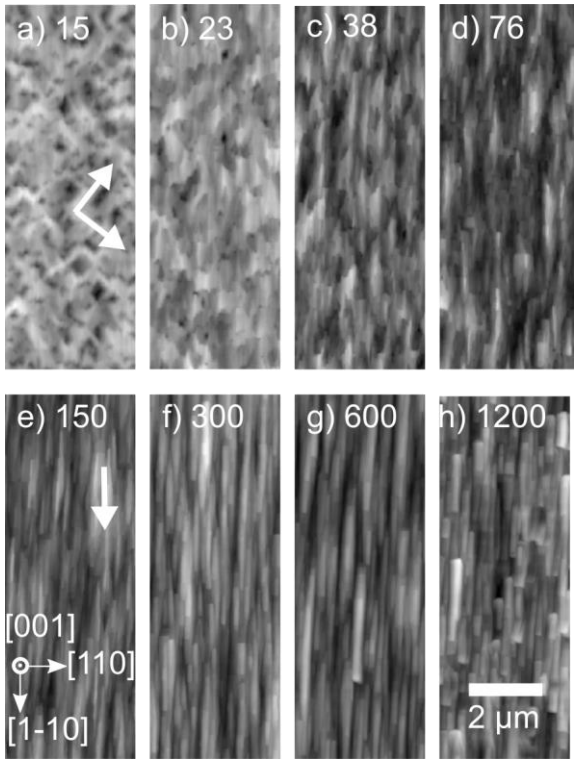

Figure 7 AFM scans of the surfaces of zb-GaN epilayers grown at various V/III-ratios and a constant growth temperature of 875 °C. The V/III-ratio used is indicated at the top of each image. From (a) – (h), H = 256 nm, 200 nm, 81 nm, 90 nm, 117 nm, 165 nm, 156 nm, 152 nm. The bold white arrows in (a) and (e) indicate the predominant in-plane orientations of the surface features.

The change in surface morphology with V/III-ratio is also apparent in the quantitative data extracted from the AFM height scans, as presented in Figure 8, which reveals three regimes that we label as i, ii and iii. It is not meaningful to extract features sizes along [110] and [1-10] in the case of the sample grown at a V/III ratio of 15 (in regime i) since for this sample

the predominant orientation of the features is along neither of these two directions which dominate the other samples.

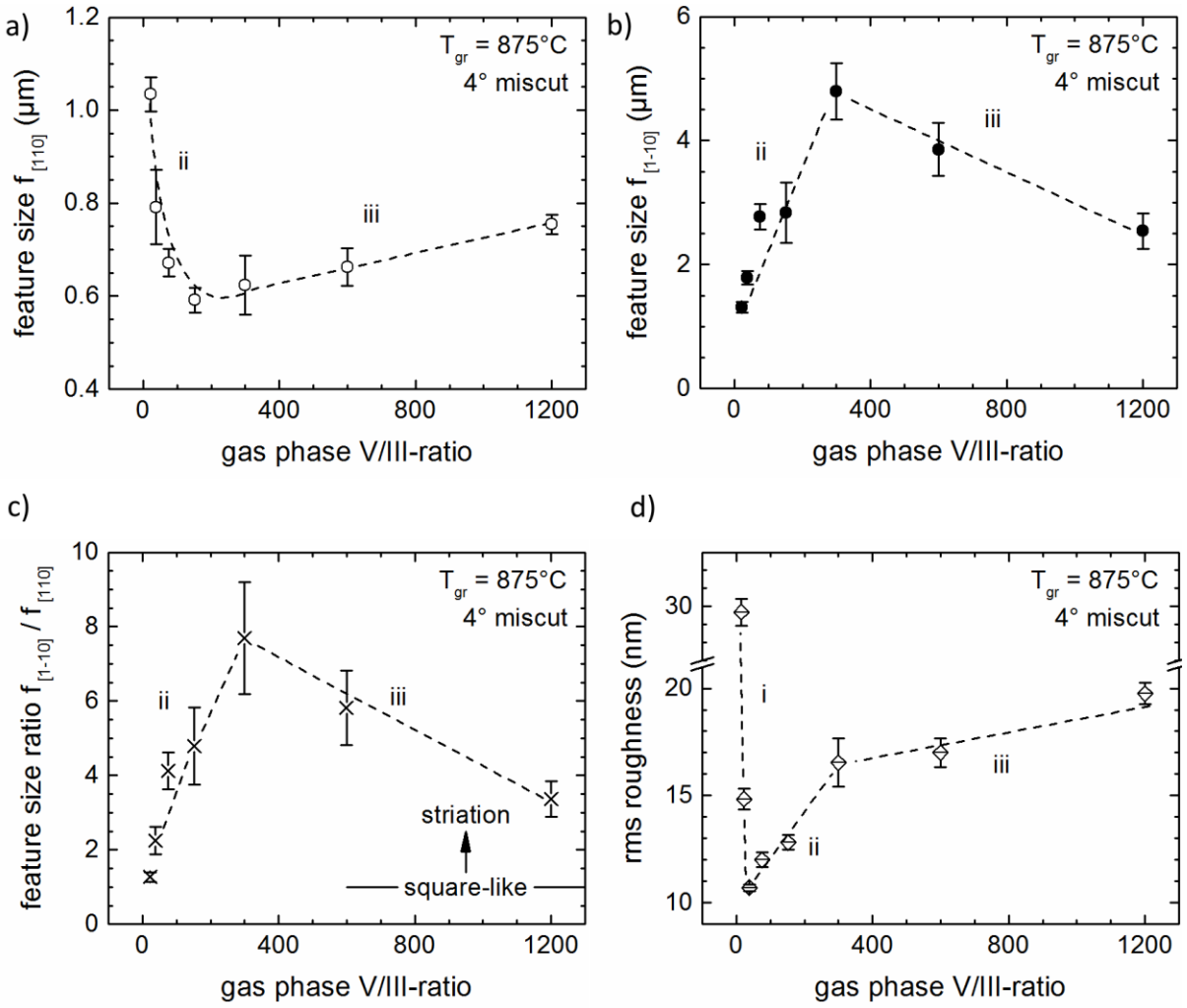

Figure 8 Feature sizes in (a) [110] and (b) [1-10] directions extracted from 2D-FFT of AFM height data of the zb-GaN epilayers grown at different V/III-ratios and a constant growth temperature of 875 °C. (c) Variation of aspect ratio of surface features with V/III ratio. For (a) to (c), there are no data points for the sample grown at a V/III-ratio of 15, as it was not possible to extract feature sizes using the same 2D-FFT method as for other sample in the series. (d) Variation of root mean square surface roughness with V/III-ratio. The labels i, ii and iii indicate the proposed growth regimes.

Regime i

The distinction between regimes i and ii is only apparent from the comparison of rms roughnesses in Figure 8 (d), and is unclear from feature sizes in Figure 8 (a) – (c). The sample grown at a V/III-ratio of 15, with the long axes of surface features at ~ ± 45° to the [110] direction (marked by the bold white arrows in Figure 9 (a)), has a particularly high rms surface roughness of (29.7 ± 0.7) nm. As the V/III-ratio increases and the surface features become increasingly aligned in [1-10] direction along the potential valleys (as discussed in Section 3.2), the rms roughness decreases to the lowest value in the series of (10.7 ± 0.1) nm at a V/III-ratio of 38. Figure 9 (b) is a 2 × 2 μm^2 AFM scan of a surface feature typically observed in the sample grown at a V/III-ratio of 15 in Figure 9 (a). Note that the fast scan direction is along [010], perpendicular to the longer facet of the surface feature. The steepest slope of several similar facets is measured to be between 45° – 55° with respect to the bottom surface of the substrate, as determined from line profiles of AFM height scans such as in Figure 9 (c). Such facet angles, together with the fact that the facets are aligned along the <100> in-plane directions, suggest that the facets observed in Figure 9 (a) are (-101), (101), (011), or (0-11) facets. From Figure 9 (b), we also note the existence of surface features with axes along [110] and [1-10], which become predominant at higher V/III-ratios in the growth regimes ii and iii. This suggests that we are approaching the point where the facet energies are approximately equal, and as we further decrease the V/III-ratio the {101}-type facets mentioned above become more prominent.

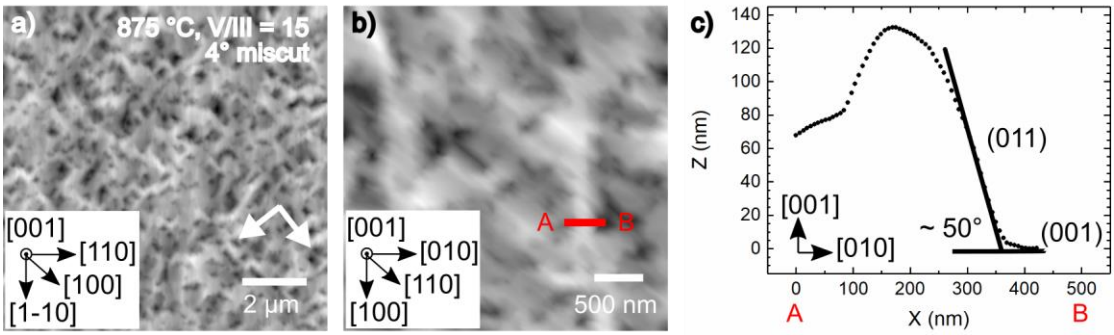

Figure 9 (a) 10 × 10 µm^2 AFM scan (fast scan direction = [110]) of the sample grown at the lowest V/III-ratio of 15 showing surface features with their long axes at ~ ± 45° to [110]. The bold white arrows on the image indicate the predominant orientations of the surface features. H = 256 nm. (b) 3.3 × 3.3 µm^2 AFM scan (fast scan direction = [010]) of a typical surface feature in (a) with its long axis at ~ + 45 ° to the [110]. H = 207 nm. (c) Line profile of the facet indicated by the red line (AB) in (b).

Regime ii

In regime ii, as the V/III-ratio increases from 38 to 300, the feature size parallel to the [110] direction ($f_{[110]}$) decreases from (0.79 ± 0.08) µm to about (0.62 ± 0.06) µm (Figure 8 (a)), while the feature size in [1-10] direction ($f_{[1\text{-}10]}$) increases from (1.78 ± 0.11) µm to (4.8 ± 0.45) µm (Figure 8 (b)). As a result, the ratio of $f_{[1\text{-}10]}/ f_{[110]}$ increases from 1.8 ± 0.1 at a V/III-ratio of 38 to a maximum of 7.7 ± 1.1 at a V/III-ratio of 300 (Figure 8 (c)). Moreover, the rms roughness increases from (10.7 ± 0.1) nm to (16.5 ± 1.1) nm with increasing V/III-ratio from 38 to 300 (Figure 8 (d)).

The feature size results indicate that the formation of the surface morphology is diffusion limited in regime ii. Since N adatoms tend to have a higher sticking coefficient on GaN surfaces than Ga adatoms [35], an increasing density of N adatoms at higher V/III-ratios inhibits diffusion across the -Ga-N- chains on the surface, along the [110] direction. Therefore

increasing the V/III-ratio in regime ii has the same diffusion-limiting effect as decreasing the growth temperature in the temperature series (Section 3.1).

The facets present in regime ii can be identified from the bright-field TEM image (zone axis = [-110], g = 111) of the sample grown at a V/III-ratio of 300 in Figure 10 (a), by measuring the angles between the facets and the {111} stacking faults, a sample of which are indicated by the white dashed lines. The TEM images in Figure 10 (a) and (b) view along the elongated features shown in the AFM scans in Figure 7 (f) and (h), respectively, and it is assumed that any projection issues can be ignored. The (001) surface is marked by the blue dotted lines; {116}, {113} and {112} facets by yellow dashed lines; and {111} facets by red dashed lines. The marked change in surface morphology between regimes i and ii can thus be explained by a change in the relative facet energies between {101} facets in regime i, and {116}, {113}, {112} and {111} facets in regime ii, although surface energies are likely to control the surface morphology in all three regimes. Despite the appearance of a range of facets, we note that the most predominant facet orientation is still (001), and that anisotropic diffusion on this facet will still be a significant factor in controlling the morphology.

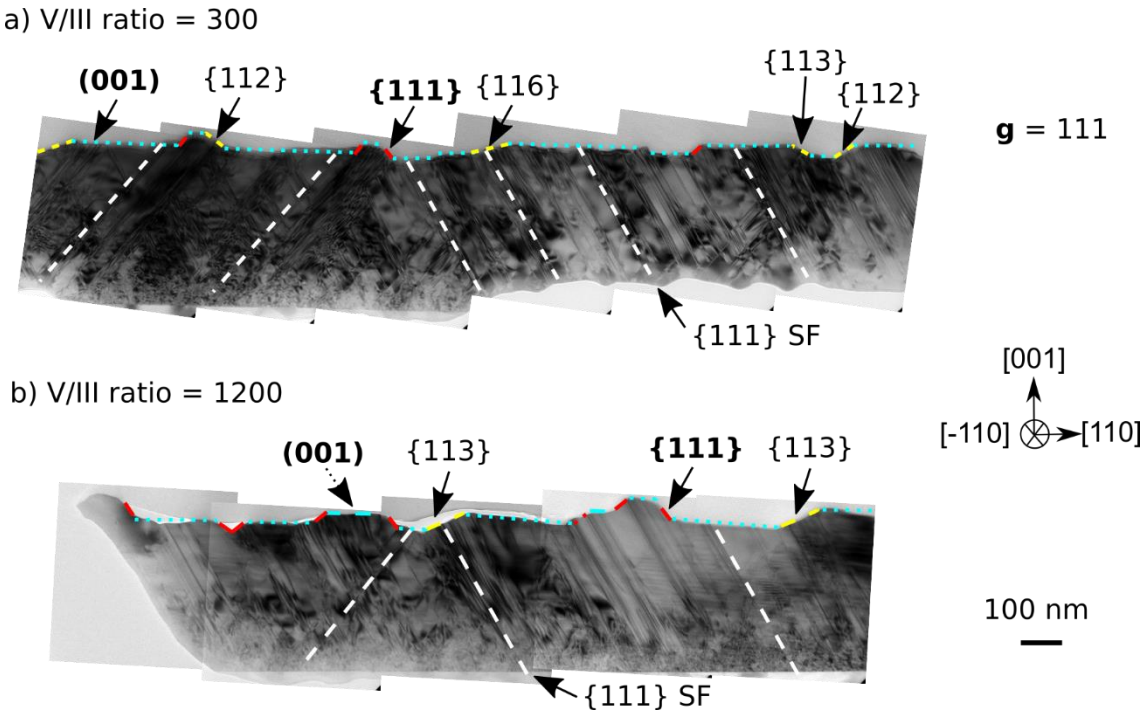

Figure 10 Bright-field TEM images of the samples grown at a temperature of 875 °C and (a) V/III-ratio of 300, (b) V/III-ratio of 1200. Imaging conditions: zone axis = [-110], g = 111. For both (a) and (b), the typical {111} stacking fault orientations are indicated by the white dashed lines, the (001) surface by the blue dotted lines, {111} facets by the red dashed lines, and other facets by yellow dashed lines. The facets in (b), the {111} facets in particular, are larger and more pronounced than in (a).

Regime iii

In regime iii, as the V/III-ratio increases from 300 to 1200, the feature size parallel to the [110] direction ($f_{[110]}$) increases from (0.62 ± 0.06) µm to (0.75 ± 0.02) µm (Figure 8 (a)), while the feature size in [1-10] direction ($f_{[1\text{-}10]}$) decreases from (4.80 ± 0.45) µm to (2.54 ± 0.29) µm (Figure 8 (b)). Hence the feature size ratio, $f_{[1\text{-}10]}/ f_{[110]}$, decreases from (7.7 ± 1.1) at V/III-ratio of 300 to (3.4 ± 0.4) at V/III-ratio of 1200 (Figure 8 (c)), displaying the opposite trend to growth regime ii. The rms roughness shown in Figure 8 (d) increases only

slightly from (16.5 ± 1.1) nm to (19.8 ± 0.5) nm, indicating a much lower dependence on the V/III-ratio.

We propose that in regime iii, the surface becomes saturated with N adatoms, therefore the diffusion limited model of regime ii breaks down. Instead the N-saturated zb-GaN surface seems to encourage the formation of {111} facets. Figure 10 (b) shows the bright-field TEM images (zone axis = [-110], g = 111) of the sample grown at the highest V/III-ratio of 1200. The (001) surface is marked by the blue dotted lines; {113} facets by yellow dashed lines; and {111} facets by red dashed lines. The sample grown at a V/III-ratio of 1200 has larger and more pronounced {111} facets compared with the sample grown at a V/III-ratio of 300 in Figure 10 (a). It is thought that the formation of such exposed {111} facets in the zb-GaN epilayer increases the likelihood for the nucleation of wurtzite inclusions, since the {111} zincblende planes and {0002} wurtzite planes differ only in their stacking sequence [36]. Hence, the {111} facets are expected to lead to the presence of a significant proportion of wurtzite phase within the thin film.

Results from XRD analysis in Figure 11 show that the proportion of the zincblende phase is between > 98 % and 100 % for the samples grown in regime i and ii. In regime iii, as the V/III-ratio increases from 300 to 1200, the proportion of the zincblende phase decreases to ~ 73 %, with increased proportions of the wurtzite phase and highly defective zb-GaN material. Such results support the view that {111} facets encourage the formation of wurtzite inclusions. Furthermore, we should note that although the two samples grown at the highest V/III-ratios of 600 and 1200 have lower zincblende phase purity, they have elongated surface morphologies similar to samples with higher zincblende phase purity. This indicates that the surface morphology is not significantly influenced by the presence of wurtzite inclusions.

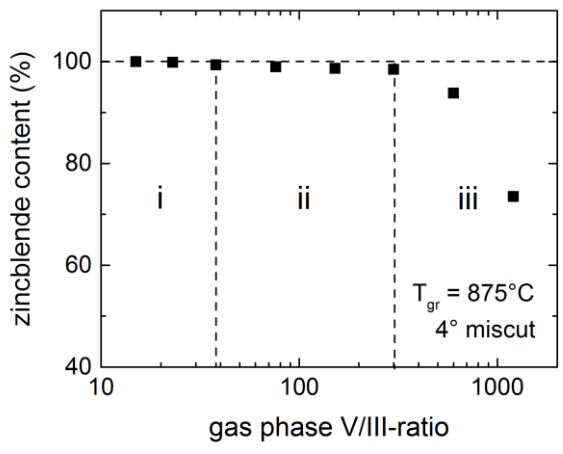

Figure 11 Relative intensities of the zb-GaN XRD peaks for samples in the V/III-ratio series at a constant growth temperature of 875 °C. The three different growth regimes are labelled with i, ii and iii.

4. Conclusion

Under a wide range of growth conditions, MOVPE-grown (001) zb-GaN thin films, with zincblende phase purity higher than 98 %, exhibit an undulating surface morphology. The surface morphology is similar for zb-GaN grown on 4° and 0° miscut substrates, which indicates that it is not determined by the step-bunching associated with the miscut. The 90° rotation of the surface morphology in neighbouring APDs of zb-GaN grown on a 0° miscut substrate further suggests that the surface morphology is controlled by the symmetry of the crystal surface. The size of the surface features and the rms surface roughness of the thin films can be controlled by the growth temperature and gas-phase V/III-ratio. The dependence on temperature indicates that the formation of such surface features is diffusion limited, which we have explained by considering the atomic structure of the zb-GaN (001) surface plane and the two-fold symmetry of the Ga-N bilayers. The dependence on V/III-ratio revealed three distinct growth regimes, of which the regime at moderate V/III-ratios (regime ii: V/III-ratio of 38 to 300) is diffusion limited. A lower V/III-ratio of 15 resulted in features

with {101}-type facets, but we do not have data available to understand the role of surface diffusion in controlling such a surface morphology. At V/III-ratios greater than 600, pronounced {111} facets are believed to increase the likelihood of formation of wurtzite inclusions. For optimised growth of zb-GaN growth with low surface roughness, we recommend a growth temperature around 885 °C and a V/III-ratio of 38 in the gas phase.

Acknowledgements

We would like to thank Innovate UK for the financial support within the Energy Catalyst Round 2 - Early Stage Feasibility scheme (Ref. 132135) and Energy Catalyst Round 4 - Mid Stage Feasibility scheme (Ref. 102766). We acknowledge the support of EPSRC through grant no. EP/M010589/1 and grant no. EP/R01146X/1. DJW would like to thank the support of EPSRC through grant no. EP/N01202X/1.

References

[1] M. Mizuta, S. Fujieda, Y. Matsumoto, and T. Kawamura, Jpn. J. Appl. Phys. **25**, L945 (1986).

[2] H. Okumura, K. Ohta, G. Feuillet, K. Balakrishnan, S. Chichibu, H. Hamaguchi, P. Hacke, and S. Yoshida, J. Cryst. Growth **178**, 113 (1997).

[3] O. Brandt, H. Yang, A. Trampert, and K.H. Ploog, Mater. Res. Soc. Symp. Proc. **395**, 27 (1996).

[4] Z.H. Feng, H. Yang, S.M. Zhagn, L.H. Duan, H. Wang, and Y.T. Wang, J. Cryst. Growth **235**, 207 (2002).

[5] D. Wang, S. Yoshida, and M. Ichikawa, Appl. Phys. Lett. **80**, 2472 (2002).

[6] D.J. As, D. Schikora, and K. Lischka, Phys. Status Solidi C Conf. **0**, 1607 (2003).

[7] D.G. Pacheco-Salazar, S.F. Li, F. Cerdeira, E. a. Meneses, J.R. Leite, L.M.R. Scolfaro, D.J.

As, and K. Lischka, J. Cryst. Growth **284**, 379 (2005).

[8] S. Li, J. Schörmann, D.J. As, and K. Lischka, Appl. Phys. Lett. **90**, 071903 (2007).

[9] S. V Novikov, N.M. Stanton, R.P. Campion, R.D. Morris, H.L. Geen, C.T. Foxon, and A.J. Kent, Semicond. Sci. Technol **23**, 15018 (2008).

[10] C.J.M. Stark, T. Detchprohm, S.C. Lee, Y.-B. Jiang, S.R.J. Brueck, and C. Wetzel, Appl. Phys. Lett. **103**, 232107 (2013).

[11] C. Bayram, J. a. Ott, K.-T. Shiu, C.-W. Cheng, Y. Zhu, J. Kim, M. Razeghi, and D.K. Sadana, Adv. Funct. Mater. **24**, 4492 (2014).

[12] M.T. Durniak, A.S. Bross, D. Elsaesser, A. Chaudhuri, M.L. Smith, A.A. Allerman, S.C. Lee, S.R.J. Brueck, and C. Wetzel, Adv. Electron. Mater. 1 (2016).

[13] T. Hanada, in *Oxide Nitride Semicond.* (Springer Berlin Heidelberg, 2009), pp. 1–19.

[14] L.Y. Lee, Mater. Sci. Technol. (United Kingdom) **33**, 1570 (2017).

[15] E. Martinez-Guerrero, E. Bellet-Amalric, L. Martinet, G. Feuillet, B. Daudin, H. Mariette, P. Holliger, C. Dubois, C. Bru-Chevallier, P.A. Nze, T. Chassagne, G. Ferro, and Y. Monteil, J. Appl. Phys. **91**, 4983 (2002).

[16] R.M. Kemper, P. Veit, C. Mietze, a. Dempewolf, T. Wecker, F. Bertram, J. Christen, J.K.N. Lindner, and D.J. As, Phys. Status Solidi **12**, 469 (2015).

[17] A. Trampert, O. Brandt, and K.H. Ploog, Angew. Chem. Int. Ed. Engl. **36**, 2111 (1997).

[18] S. Strite, J. Ruan, Z. Li, A. Salvador, H. Chen, D.J. Smith, W.J. Choyke, and H. Morkoc, J. Vac. Sci. Technol. B Microelectron. Nanom. Struct. **9**, 1924 (1991).

[19] H. Yang, O. Brandt, and K. Ploog, Phys. Status Solidi **194**, 109 (1996).

[20] S. V Novikov, N. Zainal, A. V Akimov, C.R. Staddon, A.J. Kent, and C.T. Foxon, J. Vac. Sci. Technol. B J. Appl. Phys. **28**, 3 (2010).

[21] A. Nakadaira and H. Tanaka, J. Electron. Mater. **26**, 320 (1997).

[22] J. Wu, H. Yaguchi, K. Onabe, Y. Shiraki, and R. Ito, Jpn. J. Appl. Phys. **37**, 1440 (1998).

[23] J. Wu, H. Yaguchi, H. Nagasawa, Y. Yamaguchi, K. Onabe, Y. Shiraki, and R. Ito, Japanese J. Appl. Phys. Part 1 Regul. Pap. Short Notes Rev. Pap. **36**, 4241 (1997).

[24] J. Camassel, P. Vicente, N. Planes, J. Allegre, J. Pankove, and F. Namavar, Phys. Status Solidi B-Basic Res. **216**, 253 (1999).

[25] C.H. Wei, Z.Y. Xie, L.Y. Li, Q.M. Yu, and J.H. Edgar, J. Electron. Mater. **29**, 317 (2000).

[26] M. Frentrup, L.Y. Lee, S.L. Sahonta, M.J. Kappers, F. Massabuau, P. Gupta, R.A. Oliver, C.J. Humphreys, and D.J. Wallis, J. Phys. D. Appl. Phys. **50**, (2017).

[27] I. Horcas, R. Fernández, J.M. Gómez-Rodríguez, J. Colchero, J. Gómez-Herrero, and A.M. Baro, Rev. Sci. Instrum. **78**, (2007).

[28] R.M. Kemper, T. Schupp, M. Häberlen, T. Niendorf, H. Maier, F. Bertram, J. Christen, R. Kirste, A. Hoffmann, J. Lindner, D.J. As, R.M. Kemper, T. Schupp, M. Ha, A. Dempewolf, F. Bertram, R. Kirste, and A. Hoffmann, J. Appl. Phys. **110**, (2011).

[29] S.H. Huang, G. Balakrishnan, A. Khoshakhlagh, L.R. Dawson, and D.L. Huffaker, Appl. Phys. Lett. **93**, (2008).

[30] S. Ploch, J. Bum Park, J. Stellmach, T. Schwaner, M. Frentrup, T. Niermann, T. Wernicke, M. Pristovsek, M. Lehmann, and M. Kneissl, J. Cryst. Growth **331**, 25 (2011).

[31] H. Gao and W.D. Nix, Annu. Rev. Mater. Sci. **29**, 173 (1999).

[32] L. Lymperakis and J. Neugebauer, Phys. Rev. B - Condens. Matter Mater. Phys. **79**, 1 (2009).

[33] U.W. Pohl, in *Ep. Semicond.* (Springer-Verlag Berlin Heidelberg, 2013), pp. 171–224.

[34] S. Ploch, T. Wernicke, D. V. Dinh, M. Pristovsek, and M. Kneissl, J. Appl. Phys. **111**, 10 (2012).

[35] D. Wang, Y. Hiroyama, M. Tamura, M. Ichikawa, and S. Yoshida, Appl. Phys. Lett. **76**, 1683 (2000).

[36] A. Trampert, O. Brandt, H. Yang, and K.H. Ploog, Appl. Phys. Lett. **70**, 583 (1997).